AMERICAN SOCIETY FOR MICROBIOLOGY | Journal of Virology®

VACCINES AND ANTIVIRAL AGENTS

Efficacy of Coxsackievirus A5 Vaccine Candidates in an Actively Immunized Mouse Model

Wei-Ping Jin,[a] Jia Lu,[a] Xiao-Yu Zhang,[a] Jie Wu,[a] Zhen-Ni Wei,[a] Jian-Yi Mai,[a]* Sha-Sha Qian,[a] Yu-Ting Yu,[a] Sheng-Li Meng,[a] Ze-Jun Wang,[a] Shuo Shen[a]

[a]Wuhan Institute of Biological Products, Co. Ltd., Jiangxia District, Wuhan, People's Republic of China

ABSTRACT Coxsackievirus A5 (CV-A5) has recently emerged as a main hand, foot, and mouth disease (HFMD) pathogen. Following a large-scale vaccination campaign against enterovirus 71 (EV-71) in China, the number of HFMD-associated cases with EV-71 was reduced, especially severe and fatal cases. However, the total number of HFMD cases remains high, as HFMD is also caused by other enterovirus serotypes. A multivalent HFMD vaccine containing 4 or 6 antigens of enterovirus serotypes is urgently needed. A formaldehyde-inactivated CV-A5 vaccine derived from Vero cells was used to inoculate newborn Kunming mice on days 3 and 10. The mice were challenged on day 14 with a mouse-adapted CV-A5 strain at a dose that was lethal for 14-day-old suckling mice. Within 14 days postchallenge, groups of mice immunized with three formulations, empty particles (EPs), full particles (FPs), and a mixture of the EP and FP vaccine candidates, all survived, while 100% of the mock-immunized mice died. Neutralizing antibodies (NtAbs) were detected in the sera of immunized mice, and the NtAb levels were correlated with the survival rate of the challenged mice. The virus loads in organs were reduced, and pathological changes and viral protein expression were weak or not observed in the immunized mice compared with those in alum-inoculated control mice. Another interesting finding was the identification of CV-A5 dense particles (DPs), facilitating morphogenesis study. These results demonstrated that the Vero cell-adapted CV-A5 strain is a promising vaccine candidate and could be used as a multivalent HFMD vaccine component in the future.

IMPORTANCE The vaccine candidate strain CV-A5 was produced with a high infectivity titer and a high viral particle yield. Three particle forms, empty particles (EPs), full particles (FPs), and dense particles (DPs), were obtained and characterized after purification. The immunogenicities of EP, FP, and the EP and FP mixture were evaluated in mice. Mouse-adapted CV-A5 was generated as a challenge strain to infect 14-day-old mice. An active immunization challenge mouse model was established to evaluate the efficacy of the inactivated vaccine candidate. This animal model mimics vaccination, similar to immune responses of the vaccinated. The animal model also tests protective efficacy in response to the vaccine against the disease. This work is important for the preparation of multivalent vaccines against HFMD caused by different emerging strains.

KEYWORDS CV-A5 vaccine, efficacy, active immunization, mouse model

Coxsackievirus A5 (CV-A5) is a member of species A in the genus *Enterovirus*, family *Picornaviridae* (1). Its single-stranded, positive-sense RNA genome is approximately 7,400 bases in length, with a single large open reading frame (ORF) flanked by 5′ and 3′ terminal untranslated regions (UTRs). Similar to the case with other picornaviruses, the polyprotein is cleaved by the viral proteinases $2A^{Pro}$, $3C^{Pro}$, and $3CD^{Pro}$ into viral structural, nonstructural, and intermediate proteins. The intermediate polyprotein P1 is

Citation Jin W-P, Lu J, Zhang X-Y, Wu J, Wei Z-N, Mai J-Y, Qian S-S, Yu Y-T, Meng S-L, Wang Z-J, Shen S. 2021. Efficacy of coxsackievirus A5 vaccine candidates in an actively immunized mouse model. J Virol 95:e01743-20. https://doi.org/10.1128/JVI.01743-20.

Editor Stacey Schultz-Cherry, St. Jude Children's Research Hospital

Address correspondence to Shuo Shen, shenshuo1@sinopharm.com.

* Present address: Jian-Yi Mai, Willie Russell Laboratories, University of St. Andrews, St. Andrews, United Kingdom.

Received 2 September 2020
Accepted 18 November 2020
Accepted manuscript posted online 6 January 2021
Published 24 February 2021

first cleaved into VP0, VP3, and VP1, forming an empty particle (EP) or procapsid. With the involvement of viral RNA, VP0 is autocleaved into VP4 and VP2 (2) and forms a mature, infectious, and full particle (FP) or virion. The FP is a small, nonenveloped virion that induces much stronger neutralizing antibody levels than EPs, similar to the case with other enteroviruses (3). VP1, VP2, and VP3 are located outside the virion, whereas VP4 is located inside.

The prototype Swartz strain of CV-A5 was isolated from a patient with poliomyelitis in the United States in 1950 (4). Worldwide, CV-A5 causes a variety of diseases, including HFMD, exanthema, herpangina, onychomadesis, stomatitis, and gastroenteritis (5–9), and severe cases have been reported, such as acute encephalopathy, when infected or coinfected with norovirus (10, 11). CV-A5 isolation in the spinal fluid of a patient with Reye syndrome indicated its involvement in the central nervous system (CNS) and its neurovirulence (12). Kon and colleagues reported that chronic encephalitis was associated with CV-A5, which was isolated from cerebrospinal fluid (13). Recently, it reemerged as an important etiological agent associated with HFMD in China (14).

Similar to the three previous reports (14–16), following vaccination with the EV-71 vaccine, a molecular epidemiological investigation of HFMD conducted by us in Xiangyang, China, revealed that a relatively high proportion of HFMD cases were caused by CV-A5 (unpublished data). Circulation of multiple serotypes of enteroviruses may facilitate coinfection and the emergence of new recombinants (1). The prevailing CV-A5 isolated from Xiangyang is a newly emerged recombinant carrying P2 and P3 sequences from a CV-A2 strain. This novel recombinant might be more contagious with a tendency to prevail, resulting in an epidemic outbreak.

As HFMD is caused by a variety of enterovirus serotypes, the EV-71 vaccine alone cannot prevent infection caused by other serotypes. Little, if any, cross-neutralizing activity has ever been detected, and neutralizing antibodies against one serotype cannot neutralize different serotypes (17). Therefore, multivalent vaccines containing antigens of the main serotypes are urgently needed to prevent infants and young children from becoming infected by HFMD-associated enteroviruses.

In this study, a Vero cell-derived, inactivated CV-A5 vaccine candidate was developed, and its efficacy was evaluated in a newly established mouse model. The immune response was stimulated by priming and boosting with the vaccine candidate, and the survival rate was 100% following virus challenge at a lethal dose. The survival rate of immunized mice correlated with high levels of neutralizing antibodies and decreased viral loads in organs. The immunogenicity of EPs and FPs of CV-A5 was also compared in this study. Dense particles (DPs) were also isolated and characterized. The promising CV-A5 vaccine candidate could be used as one of the components in a multivalent vaccine against HFMD if needed.

RESULTS

Preparation of a vaccine candidate. In an outbreak of HFMD in Xiangyang, China, in 2017, rectal swabs from patients were obtained. CV-A5-3487 was isolated in both RD and Vero cells and grown to titers higher than 1×10^8 50% cell culture infectious doses ($CCID_{50}$)/ml. A Vero cell isolate, CV-A5-vN20, was selected as a vaccine candidate. Vero cells in a 10-layer cell factory were infected with CV-A5-vN20 at a multiplicity of infection (MOI) of 0.001. The harvest was purified through two steps of ultracentrifugation. Three bands produced by ultracentrifugation in a CsCl gradient were collected and designated EPs (1.29 g/ml), FPs (1.33 g/ml), and DPs (1.44 g/ml), as shown in Fig. 1A. The percentages of EPs, FPs, and DPs accounted for 20%, 70%, and 10%, respectively.

EPs were composed of VP0, VP1, and VP3 and FPs consisted of VP1 to VP4, while DPs contained VP1, VP2, and VP3 (Fig. 1B). The identities of these structural proteins were confirmed by Western blotting using homemade rabbit anti-VP1, anti-VP2, anti-VP3, anti-VP4, and anti-FP antisera (Fig. 1C). For EPs, VP2 as well as VP0, VP1, and VP3 were detected. The results suggested the presence of two kinds of empty particles,

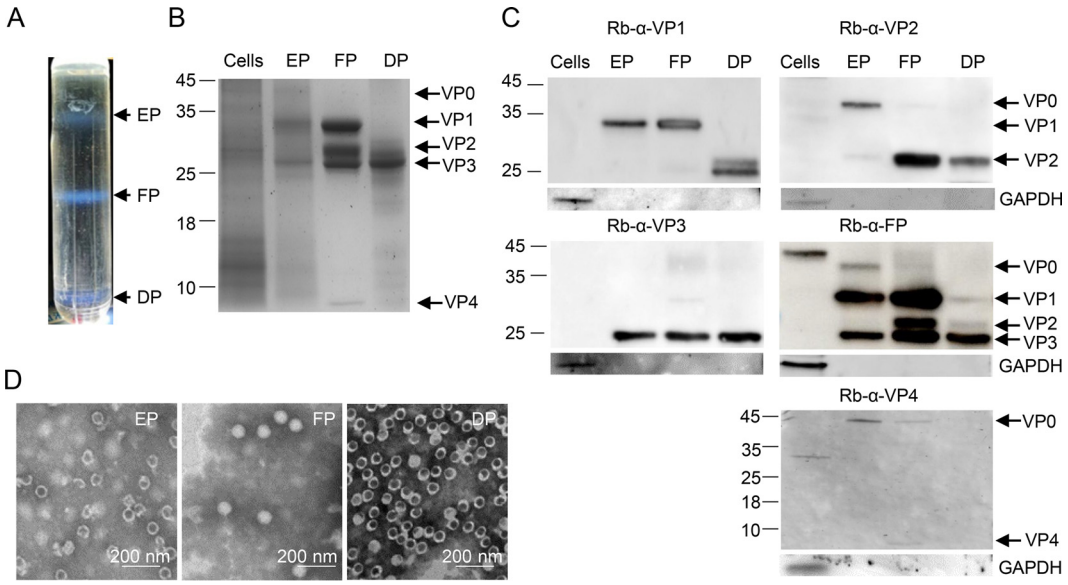

FIG 1 CV-A5 purification and identification. CV-A5 particles were harvested from infected Vero cells and purified by CsCl gradient ultracentrifugation. (A) The positions of empty, full, and dense particles (EPs, FPs, and DPs) are indicated. (B) The mock-infected Vero cell, EP, FP, and DP bands were subjected to SDS–4 to 20% PAGE and stained with Coomassie brilliant blue. (C) Proteins of the EPs, FPs, DPs, and mock-infected Vero cells were detected by Western blotting using the antibodies indicated at the top of each panel. VP0, VP1, VP2, VP3, and VP4 are indicated with arrows on the right, and molecular weight markers, in kilodaltons, are indicated with lines on the left. (D) The purified EPs, FPs, and DPs were inactivated with formaldehyde and examined by transmission electron microscopy. Scale bar, 200 nm.

those following the release of viral RNA in the cell entry step and procapsids with an uncleaved VP0. An antibody against the virion did not recognize VP4. EPs banded at a density of 1.29 g/ml in the CsCl gradient. For FPs, VP1, VP2, VP3, and VP4 were detected, indicating that they were native and mature particles. The mature virion also contained a few uncleaved VP0 molecules, as reported previously for CV-A16 (3). A small portion of FPs contained procapsids, and VP4 was detected, while EPs and DPs did not contain VP4 (Fig. 1B), which was supported by transmission electron microscopy (TEM) examination (Fig. 1D). For DPs, the protein profile showed that the bands of VP1 were faint and small, and degradation products were observed (Fig. 1C); VP2 and VP3 showed similar results, suggesting the sensitivity of these particles to cellular proteases. The sizes of the three particles were examined under an electron microscope. The diameters of EPs, FPs, and DPs were 25 ± 2 nm ($n = 110$), 25 ± 3 nm ($n = 114$), and 28 ± 3 nm ($n = 550$), respectively, by measuring more than 100 particles of each form (Fig. 1D).

Immunogenicity and immune persistence of the CV-A5 vaccine. The immunogenicities of the purified EPs, FPs, and an EP and FP mixture (abbreviated EP+FP; natural particle ratio, 2:8) were tested in 6-week-old BALB/c female mice to study the dose-dependent effects of the three formulations, as shown in Fig. 2.

For the three formulations, significant differences following priming and boosting were observed (Fig. 2A to C). For EPs, there were significant differences in NtAb levels between the low (0.5 μg) and median/high (1.5 and 4.5 μg) doses (Fig. 2A). For FPs and EPs+FPs, the differences in the NtAb levels were not significant at the high, median, and low doses (Fig. 2B and C).

Significant dose-dependent effects were observed for the EP groups, as high levels of NtAb were stimulated when doses of 1.5 or 4.5 μg per mouse were compared with those of 0.5 μg (Fig. 2D). The FPs and EP+FP mixture stimulated significantly higher ($P < 0.05$) levels of NtAb than the EPs. There was no significant difference in NtAb levels between mice stimulated with FPs and those stimulated with EPs+FPs. The induced humoral immunity was specific, as NtAbs of the mock-immunized mice were not

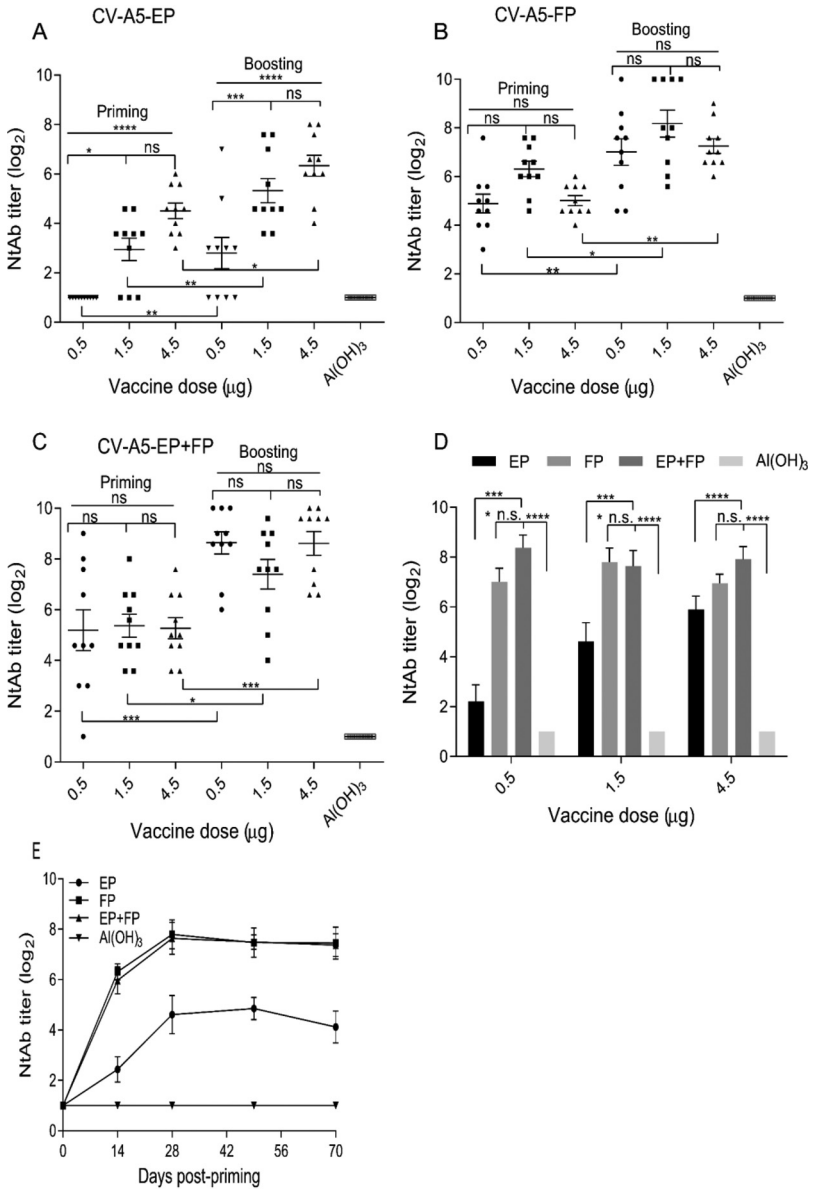

FIG 2 Humoral immune response and persistence of the three formulations. Six-week-old BALB/c mice were primed and boosted intraperitoneally on days 0 and 14 with EPs, FPs, and EPs+FPs at doses of 0.5 μg, 1.5 μg, or 4.5 μg per injection. Bleeding was performed on days 14, 28, 49, and 70. For dose-dependent effects, NtAb titers were determined by using antisera collected on day 28. (A to C) The NtAb titers induced by EPs (A), FPs (B), and EPs+FPs (C) were determined. (D) NtAb levels induced by the three formulations at the three doses were compared. (E) For immune persistence, NtAb levels were analyzed at a dose of 1.5 μg/injection at 70 days postpriming. Two-way ANOVA was used for statistical significance analysis. Titers are presented as the means ± standard errors of the means (SEM). *, $P < 0.05$; ****, $P < 0.0001$; n.s., not significant. Ten mice were used in each group. Immunization doses are indicated in panels A, B, and C. NtAb titers below 8 were assigned to 2 for the convenience of presentation.

detectable. NtAb levels remained high for the FP and EP+FP groups on days 49 and 70 postpriming, indicative of excellent immune persistence, in contrast to those of the EP group (Fig. 2E). Cross-neutralizing activities of induced antisera were determined against EV-71 and the CV-A5 prototype Swartz strain (Table 1). The antisera neutralized the CV-A5 prototype Swartz strain *in vitro*, which is the most genetically distant subgroup within the serotype. The results demonstrated the broad spectrum of neutralizing activity

TABLE 1 Cross-neutralizing activity of antisera

Strain	Mouse serum	Titer
EV-71 wild type	α-EP	<8
	α-FP	<8
	α-EP+FP	<8
CV-A5 prototype	α-EP	1,024
	α-FP	1,024
	α-EP+FP	1,024
CV-A5-3487-C0	α-EP	1,024
	α-FP	1,024

against the same serotype, warranting further investigation. There was no cross-neutralizing activity against a different serotype, EV-71, under the conditions of this experiment.

Establishment of a mouse model for active immunization and challenge. To establish an active immunization challenge model to evaluate the efficacy of the vaccine candidate, parental CV-A5 was used to inoculate 1-day-old mice via the intracranial (i.c.) route. The brain homogenates of severely ill mice then were prepared and passaged once in RD cells to obtain virus stock with high titers. The adaptation was performed repeatedly by sequential inoculation of 1-, 3-, 5-, 7-, 9-, 10-, 12-, and 14-day-old mice. Viral stocks were then established and propagated in RD cell cultures. Finally, a mouse-adapted virus stock, CV-A5-M14, was obtained, which caused 100% morbidity and mortality in 14-day-old mice when they were infected via either the i.c. or intraperitoneal (i.p.) route and in 7-day-old mice via oral infection.

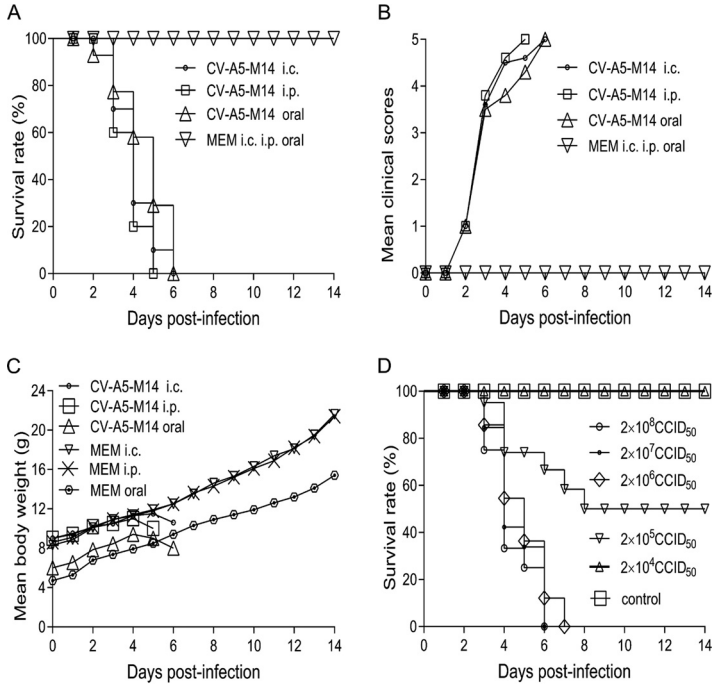

FIG 3 Virulence of CV-A5-M14 and establishment of the Kunming mouse model. CV-A5-M14 is a virulent, mouse-adapted strain that can infect 14-day-old (i.c. and i.p. routes) and 7-day-old (oral) Kunming mice. The criteria of clinical scores of infected Kunming mice are the following: 0, healthy; 1, fatigue or sleepiness; 2, weight loss and hunched back; 3, hindlimb weakness or jitter; 4, limb paralysis; 5, dying or death. The survival rates (percent) (A), mean clinical scores (B), and mean body weights (C) were compared in mice infected with CV-A5-M14 and mock-infected mice via the i.c., i.p. (14-day-old mice), and oral (7-day-old mice) routes at doses of 3×10^7 $CCID_{50}$, 3×10^8 $CCID_{50}$, and 3×10^8 $CCID_{50}$, respectively. (D) The LD_{50} of CV-A5-M14 was determined through the i.p. route at the doses indicated. The results are presented as the means ± SEM.

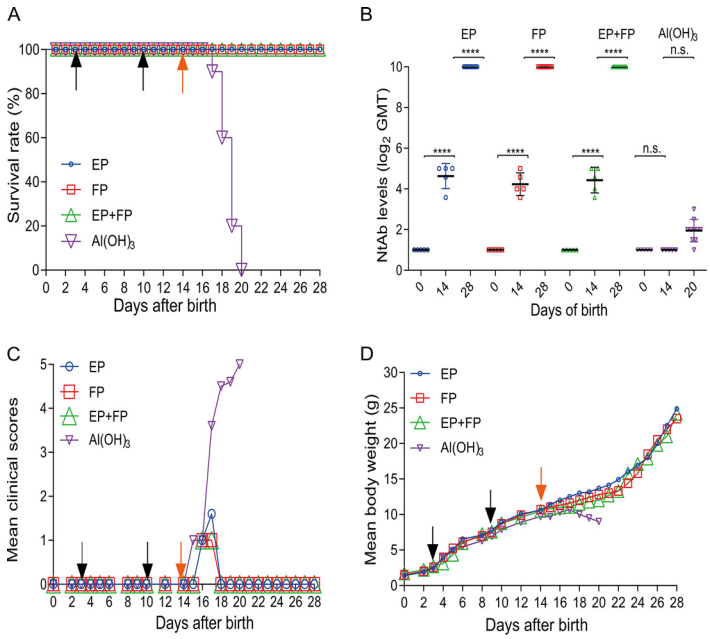

FIG 4 Efficacy of the vaccine in mice immunized with the three vaccine formulations. Kunming mice were primed and boosted on days 3 and 10 at a dose of 1.5 μg/injection and challenged at a dose of 10 LD_{50} (2×10^6 $CCID_{50}$/mouse) on day 14. (A) The survival rate (percent) was calculated 14 days postchallenge. Bleeding was performed on days 0, 14, and 28. NtAb titers of sera of mice vaccinated with EPs, FPs, EPs+FPs, or $Al(OH)_3$ ($n = 5$ for each group) were determined. NtAb titers on day 28 in mice infected with EPs, FPs, or EPs+FPs ($n = 10$ for each group) were determined. NtAb titers are presented as the means ± SEM. ****, $P < 0.0001$; n.s., not significant (by two-way ANOVA). (B) NtAb titers below 8 were assigned to 2 for the convenience of presentation. Mean clinical scores (C) and mean body weight (D) were recorded during the 14-day observation period. Black arrows indicate the date of vaccination. Orange arrows indicate the day of challenge.

As shown in Fig. 3A, inoculation via the i.c. and i.p. routes (14-day-old mice) or oral route (7-day-old mice) caused 100% fatality on day 5 or 6 at doses of 3×10^7 $CCID_{50}$ (i.c.), 3×10^8 $CCID_{50}$ (i.p.), and 3×10^8 $CCID_{50}$ (oral), respectively. In contrast, 100% of mock-inoculated mice survived for 14 days postinoculation with medium. The clinical scores of the challenged groups were higher than those of the mock-inoculated group (Fig. 3B). The body weights of the infected groups dropped quickly on day 4 or 5 postinfection compared with that of the mock-infected group (Fig. 3C). The results indicated that CV-A5-M14 could cause severe symptoms in 14-day-old mice and lead to death, providing a time window for priming and boosting newborn mice with the CV-A5 vaccine candidate before challenge to evaluate its efficacy. The i.p. route was a more effective route of infection, as a higher dose could be used. The 50% lethal dose (LD_{50}) of CV-A5-M14 via the i.p. route was 2×10^5 $CCID_{50}$/300 μl/mouse (Fig. 3D).

Efficacy of the vaccine candidate in Kunming mice. The efficacies of EPs, FPs, and EPs+FPs were evaluated at a dose of 1.5 μg/injection using CV-A5-M14 as a challenge strain at a lethal dose, as shown in Fig. 4. To reduce the nonspecific death rate and increase the defensive immune response, a group of 3-day-old mice were primed and boosted on day 10 through the i.p. route and challenged 4 days later (once antibody levels had increased) with CV-A5-M14 at a dose of 10 LD_{50} (2×10^6 $CCID_{50}$/mouse). All mice in the immunized groups survived after 14 days of observation, showing 100% protection, while all mice in the mock-immunized group died at 6 days postchallenge (Fig. 4A). Levels of NtAb titers in sera on days 0, 14, and 28 were determined, representing those of preimmunization, postboost, and postchallenge antisera (Fig. 4B). In suckling mice, NtAbs were detectable only after boosting (day 14), and the seroconversion rate was 100%. NtAb titers increased dramatically after challenge (day 28, $P < 0.001$), reflecting strong immune responses following challenge. The results demonstrated

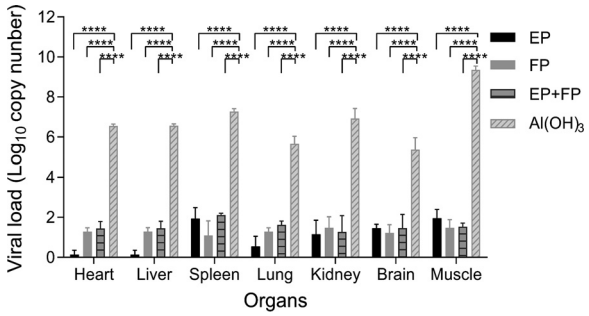

FIG 5 Viral loads in organs in intraperitoneally immunized and challenged Kunming mice. Kunming mice immunized with EPs, FPs, or EPs+FPs or mock immunized were challenged with CV-A5-M14 at a dose of 10 LD_{50} (2×10^6 $CCID_{50}$/mouse). Heart, liver, spleen, lung, kidney, brain, and muscle tissues were retrieved for sample processing. Viral loads in organs were quantitated by qRT-PCR. The data were analyzed with two-way ANOVA. The results are presented as the means ± SEM. ****, $P < 0.0001$ (versus control treatment [by two-way ANOVA]).

that NtAb levels correlated with the survival of immunized mice, and there were no differences in titers of different antigen groups. There were no significant differences in clinical scores or body weight changes between immunized and alum-inoculated mice before challenge, indicating tolerance of mice to the vaccine (Fig. 4C and D). After challenge, body weight dropped, and clinical scores increased sharply for alum-inoculated mice compared with those for mice in the three immunized groups.

Viral loads in different organs of the immunized-challenged mice. To investigate the mechanism of the protection of the vaccinated mice, the genome copy numbers in the heart, liver, spleen, lung, kidney, brain, intestine, and muscle of infected mice were determined by quantitative real-time PCR (qRT-PCR). As shown in Fig. 5, viral RNAs of immunized-challenged mice detected on day 14 postchallenge in all these organs were far below those of alum-inoculated mice on days 3 to 6 postchallenge before they died ($P < 0.0001$). The viral loads of the tested organs were decreased in the order of muscle, spleen, kidney, liver, heart, lung, and brain. It was noted that no viral RNAs were detected in the intestines (data not shown) due to the challenge via the i.p. route, not the oral route. However, viral RNAs were detected in the intestines of mice immunized with only alum. Immunization of mice with the different formulations of vaccine candidates significantly decreased the virus loads in various organs following challenge with CV-A5-M14.

Histopathologic and IHC analyses. To study virus propagation and pathogenesis, histopathological changes and immunohistochemistry (IHC) analysis were performed in vaccinated or alum-inoculated mice. All mice in the alum-inoculated group showed evidence of severe damage, including cellular infiltration, and viral proteins were highly expressed in the brain (Fig. 6B). Additionally, viral protein was detected in the lung, brain, heart, and muscle in hindlimb-paralyzed mice. All animals in the immunized groups survived without severe symptoms, and low or mild clinical scores were observed during only the first 4 days (Fig. 6A). The levels of viral protein expression in the lungs, brains, hindlimb muscles, and hearts of all immunized-challenged mice were lower than those in the alum-inoculated and challenged mice (Fig. 6B). The severity of histopathological lesions and the expression level of viral protein correlated well with the clinical scores.

DISCUSSION

Great efforts have been made to establish animal models of enteroviruses to study the pathogenesis and efficacy of vaccines and antiviral reagents. For EV-71, nonhuman primate, gerbil, and mouse models were established (18, 19). Mouse models have been established using different mouse species, immunodeficient mice, and receptor-transgenic mice. The challenging viruses were obtained from either clinical isolates or mouse-adapted strains (19–22). For other enteroviruses closely associated with HFMD,

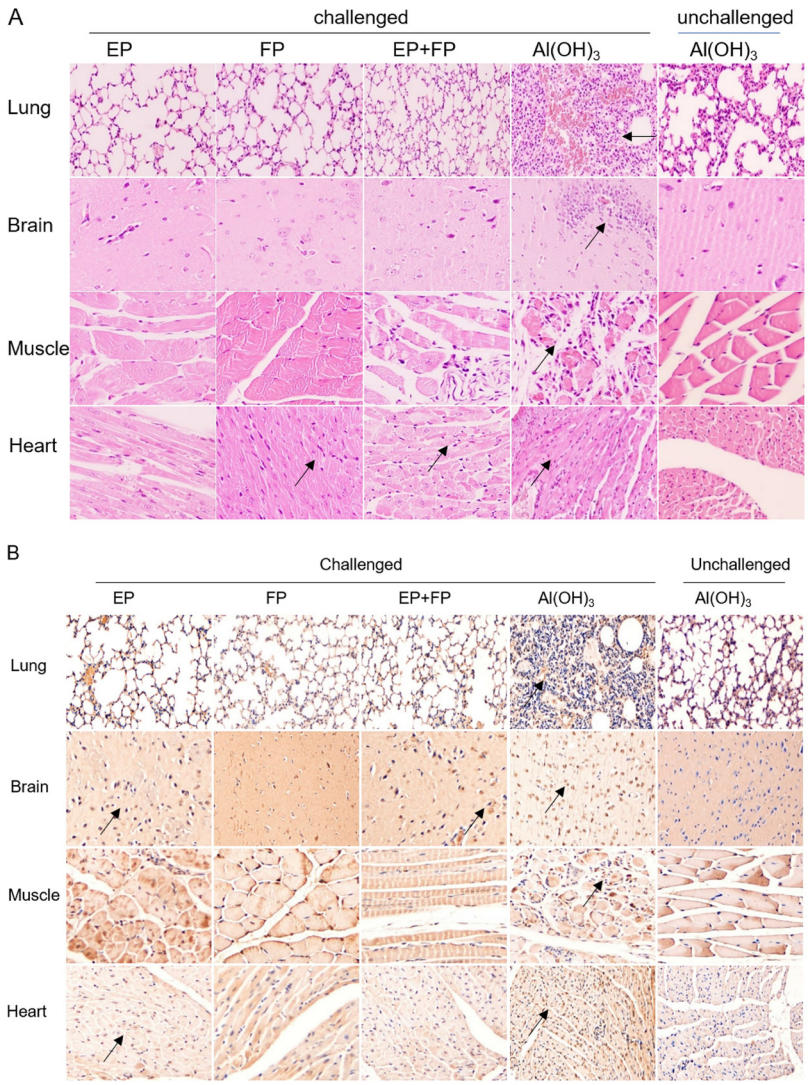

FIG 6 Pathological changes and IHC in immunized-challenged Kunming mice. Histopathological changes (A) and expression of viral protein (B) in immunized-challenged Kunming mice were analyzed. Immunized Kunming mice were challenged via the i.p. route at 2×10^6 $CCID_{50}$ with CV-A5-M14. The $Al(OH)_3$ groups were euthanized on day 6 postinfection, and mice in the vaccinated groups were euthanized at 14 days postinfection. Sections from lung, brain, muscle, and heart tissues were stained with hematoxylin to detect pathological changes. Viral proteins were detected in IHC assays with an anti-CV-A5 FP antibody, and sections were counterstained with hematoxylin. Original magnification, $\times$200.

mouse models have also been reported for CV-A16, -A6, -A10, and -A4. However, the challenging viruses that have been used infected only suckling mice younger than 3 to 5 days. Therefore, efficacy evaluations of vaccine candidates were performed via passive immunization and challenge (23–31). Suckling mice older than 3 or 5 days are not liable to infection with wild-type coxsackievirus species A and B. There are time windows to perform priming, boosting, and challenging by using our mouse-adapted strain.

Different animal models have advantages and disadvantages for different reasons (18). However, mouse models using mouse-adapted viruses to infect older suckling mice are practically useful in evaluating the efficacy of a vaccine candidate, particularly when the mice can be inoculated via the oral route. For this kind of model, as mice older than 2 weeks can be infected, it provides a time window for priming and boosting before the challenge. This active immunization-challenge model mimics

vaccination, immune responses, and immune memories of animals and protection of the vaccinated animals from diseases when challenged in a natural infection manner. In this study, a mouse-adapted strain was used to evaluate the efficacy in mice via the i.p. route, and the results indicated that a Vero cell-derived, inactivated CV-A5 was an excellent vaccine candidate, strongly supporting clinical trials for the vaccine candidate. Unfortunately, CV-A5-M14 could only cause the death of 7-day-old mice at a dose of 3×10^8 $CCID_{50}$ in oral infection; hence, this route was not suitable for efficacy evaluation. Further work is needed to map the virulence epitopes and study the neurovirulence epitopes of CV-A5. Importantly, an oral infection mimics the natural pathway of virus entry, and it can be used to investigate how an enterovirus progressively invades different organs and the CNS. This aspect makes it useful for pathogenesis study. Additionally, the relevance of neurovirulence epitopes of mouse-adapted strains to those of clinical strains should be further mapped and investigated.

After centrifugation of CV-A5-vN20 in a CsCl gradient, an extra band referred to as DPs appeared apart from the two common bands, which represented EPs and FPs (1.29 and 1.33 g/ml). The density of DPs was 1.44 g/ml, as the permeability increased and allowed Cs^+ ions to enter the particles. Previous studies on polioviruses demonstrated that there were dense particles (DPs; or dense components) in the CsCl gradient with a density of 1.44 g/ml (32, 33). These DPs were separated into two components following sucrose gradient centrifugation containing 1.5 M KCl, and they had sedimentation coefficients of 160 S and 220 S, respectively. The 160 S particle represented the native virion, and the 220 S particle was an intermediate form of the particles, probably before viral RNA was released. The 220 S dense particles were less stable, infectious, and sensitive to cellular proteinases and RNase (34, 35).

The EPs, FPs, and DPs of CV-A5 are equivalent to the 80 S, 160 S, and 220 S fractions in the sucrose gradient previously reported for polioviruses (36). The DPs contained VP1, VP2, and VP3 but not VP4, which correlates with the same components as the A particles reported by others but differs from A particles in density (36–38). Further detailed study on the components of DPs is needed. It is interesting that VP1 in DPs was truncated, using antibodies against these structural proteins. One of the explanations for this phenomenon is that the extended N-terminal region of VP1 in the entry and uncoating processes was sensitive to cellular proteinases. It is still not clear whether it is an intermediate particle between the 135 S A and 80 S empty particles that was formed before and after viral RNA release, respectively. Further detailed investigation of the dense particles as well as EPs and FPs should be performed to study morphogenesis and conformational changes during CV-A5 receptor binding and cell entry.

Immunogenicity analysis demonstrated that the FPs were stronger than EPs in terms of NtAb stimulation and immune persistence, similar to the C and D antigens of polioviruses (3). Other HFMD-associated enteroviruses have shown this characteristic. The ratio of EP and FP was more likely related to serotypes or even genotypes within the same serotype and less related to different processes of vaccine production based on our work on EV-71, CV-A2, -A5, -A6, -A10, and -A16 (unpublished data). The EPs of CV-A5 stimulated NtAb responses and could be copurified as a mixture of EPs+FPs for a vaccine candidate, as shown in this study. The detection of the ratio could be used as a quality control for vaccine production.

In conclusion, the broad cell tropism of the CV-A5 isolate with high titers used in this study provided excellent opportunities to prepare vaccine candidates and to establish animal models of infection through different routes. It also allowed the isolation of intermediate particles in the processes of morphogenesis. If CV-A5 is to be included in a multivalent vaccine in the future, these studies will greatly facilitate the development of CV-A5 vaccine candidates.

MATERIALS AND METHODS

Ethics statement. This study protocol was approved by the Animal Ethics Committee of the Wuhan Institute of Biological Products (WIBP) (WIBP-AII no. 382019005, 382019006, 382019007, and 382019008). All experiments were performed in accordance with the relevant guidelines and regulations in China (39).

Cells and viruses. African green monkey kidney (Vero) cells were cultured in Dulbecco's modified Eagle medium (DMEM; Thermo Fisher Scientific, USA) supplemented with 10% newborn bovine serum (NBS). Human rhabdomyosarcoma (RD) cells were cultured in minimal essential medium (MEM; Nissui, Japan) supplemented with 10% NBS. CV-A5-3487-M14/XY/CHN/2017 (abbreviated CV-A5-M14; GenBank accession number MW079817) and CV-A5-3487-C0/XY/CHN/2017 (abbreviated CV-A5-C0) were propagated in RD cells. Parental CV-A5 (GenBank accession number MN663160) was isolated and cultured in RD cells first. After passaging in RD cells 16 times, the isolate was adapted to grow in Vero cells. Plaque purification was performed, and a plaque-purified clone was named CV-A5-3487-vN20/XY/CHN/2017 (abbreviated CV-A5-vN20). CV-A5-vN20 was propagated in Vero cells in a 10-layer cell factory. All CV-A5 strains were isolated from specimens of HFMD patients in Xiangyang, China, in our laboratory in 2017. The virus stocks were titrated by microtitration assays and expressed as 50% of the cell culture infection dose ($CCID_{50}$) per milliliter. It was calculated using the Reed-Muench method and expressed as the reciprocal of the highest virus dilution at which cytopathic effect (CPE) in 50% of the wells was observed.

Virus purification. For the preparation of vaccine candidates, infected Vero cells in a 10-layer cell factory were freeze-thawed three times in the presence of 0.1% Tween 20 for harvesting (40). The harvest was cleared by centrifugation at 4,000 $\times$ *g* in a Beckham JA10 rotor for 30 min at 4°C. The supernatant was concentrated by ultrafiltration using a 100-kDa tangential flow filter capsule (Sartorius, Germany) to one-tenth the harvest volume. The concentrate was centrifuged through 3 ml of a 30% (wt/vol) sucrose cushion in a Beckman SW28 rotor at 103,745 $\times$ *g* for 3 h at 4°C. The pellets were resuspended in 10 mM phosphate-buffered saline (PBS) containing 0.1 mM $CaCl_2$ at 4°C overnight. The viruses were further purified by CsCl density gradient ultracentrifugation to equilibrium at a starting density of 1.31 g/ml, prepared in PBS–1 mM $MgCl_2$ in a Beckman SW41 rotor (Beckman, USA) at 150,000 $\times$ *g* for 18 h at 4°C. EP, FP, and DP fractions were collected by puncturing the side of the tube and diluting with PBS. CsCl was removed by centrifugation at 260,000 $\times$ *g* for 3 h at 4°C. Pellets were resuspended in PBS. The total protein concentrations of individual fractions were determined by Pierce bicinchoninic acid protein assay (Thermo Fisher Scientific, USA). The EP/FP natural ratio was calculated by the total mass and molar ratios, which were determined by BCA, and by the ratio of VP1 (or VP3) between EPs and FPs collected in a CsCl gradient.

Generation of antisera against the virion and structural proteins. The cDNAs of the genes encoding the structural proteins VP1 (ΔN56-253), VP2 (ΔN119-191), VP3 (ΔN8-150), and VP4 (full length) were cloned into the pGEX-6p-1 plasmid and expressed as fusion proteins in *Escherichia coli* with a glutathione *S*-transferase tag at the N terminus. CV-A5 was propagated in Vero cells, and the virions were purified. Japanese long-eared white rabbits were primed and subcutaneously boosted with purified fusion proteins and virions (41). Freund's complete adjuvants were used to emulsify the antigens for the first and second immunizations. Freund's incomplete adjuvants were used for subsequent enhancing immunizations (42). The rabbits were sacrificed 10 days after the last boosting, and antisera were collected, inactivated at 56°C for 30 min, and stored at −80°C.

Adaptation of CV-A5 to infect 2-week-old mice. The CV-A5 parental strain was inoculated in newborn Kunming mice via the intracranial (i.c.) injection route. Brain homogenates of severely ill, 1-day-old mice were prepared. Propagation in RD cells was performed once, and then inoculation of mice was performed. The process was repeated to adapt viruses to older mice aged 3, 5, 7, 10, 12, and 14 days. This process was repeated until the virus could cause death of 14-day-old mice via the i.c. and intraperitoneal (i.p.) injection routes, and CV-A5-M14 was obtained. CV-A5-M14 was purified by the plaque-to-plaque technique 3 times in RD cells for selection of clones with strong virulence.

TEM. Carbon-coated copper grids (200 mesh) were soaked with a drop of purified particles for 5 min, stained with a drop of 1% phosphotungstic acid, pH 7.0, for 5 min, and air dried overnight. The grids were viewed under transmission electron microscopy (TEM) (HITACHI, Japan), and the images were photographed. The sizes of EPs, FPs, and DPs were measured by using Nano Measurer 1.2 software.

SDS-PAGE and Western blotting. Proteins of purified CV-A5 particles or infected-cell lysates were separated by SDS-PAGE and were either stained with 0.25% Coomassie brilliant blue or transferred onto nitrocellulose membranes. The membranes were blocked overnight at 4°C in PBS containing 1% bovine serum albumin (BSA) and 0.05% Tween 20 (PBST-BSA). Each membrane strip was incubated with individual rabbit antiserum raised in immunized rabbits at room temperature for 1 h. The dilutions of six rabbit anti-VP1, anti-VP2, anti-VP3, anti-VP4, anti-FP, and anti-glyceraldehyde-3-phosphate dehydrogenase (GAPDH) antisera (Abcam, UK) were 1:7,000, 1:2,000, 1:7,000, 1:400, 1:15,000, and 1:1,500, respectively. A horseradish peroxidase (HRP)-conjugated goat anti-rabbit secondary antibody (BSD, China) was added at a dilution of 1:5,000 in PBST-BSA and incubated for 1 h. The membranes were washed three times with PBST-BSA after each incubation step. The protein bands were visualized by adding 3,3-diaminobenzidine (DAB)-substrate solution or detected with an ECL detection system (Gene, USA).

NtAb assay. Viruses were diluted in MEM so that 50 μl of the virus suspension contained 100 $CCID_{50}$. Equal volumes (50 μl) of 2-fold, serially diluted antiserum were added to virus suspensions (2 duplicates for each dilution) in 96-well plates. After incubation at 37°C for 2 h, 1×10^5 RD cells in 100 μl of MEM were added per well. Cell and serum controls were included, and virus back-titration was performed. The virus titers were in the range of 32 to 320 $CCID_{50}$/50 μl. Seven days later, the neutralizing titer was calculated using the Reed-Muench method and expressed as the reciprocal of the highest serum dilution at which CPE in 50% of the wells was completely inhibited.

Immunogenicity and efficacy in mice. The purified FPs and EPs were inactivated with commercially supplied formaldehyde at a dilution of 1:2,000 at 37°C for 96 h. To validate inactivation, inactivated particles were blindly passaged 3 times in Vero cells, and potential CPE was checked.

Neutralizing activity. Newborn Kunming mice were immunized intraperitoneally with 0.1 ml of EPs, FPs, or the EP and FP mixture (abbreviated EP+FP) on days 3 and 10. Mice were euthanized, and sera were collected on day 14 for NtAb assays. For efficacy evaluation, the immunized and alum-inoculated groups of mice were challenged intraperitoneally with CV-A5-M14 at a dose of 2×10^6 $CCID_{50}$. The mice were observed daily for 14 days for clinical symptoms, such as body weight loss, hindlimb paralysis, eye irritation, loss of balance, and death. The heart, liver, spleen, lung, kidney, brain, muscle, and intestine were fixed with 4% paraformaldehyde and embedded in paraffin for histopathology examination.

qRT-PCR. The tissues and organs of mice were collected for detection of viral loads. The copy numbers of viral RNA (vRNA) were determined by qRT-PCR using *in vitro*-transcribed RNA standards. RNA standards (10^{10} to 10^3 copies) were transcribed from the VP1 gene cloned into a plasmid. VP1 regions were used to design oligonucleotide primers and hydrolysis probes with Primer Select (Primer Premier 5.0). The hydrolysis probe was labeled with a fluorescent dye (6-carboxyfluoroescein [FAM]) and a nonfluorescent black hole quencher (BHQ) at the 5′ and 3′ ends, respectively. The forward primer CV-A5-F (5′-CAAGCTGGAAATGTTCAC), reverse primer CV-A5-R (5′-GGGTGGAACATACATGTA), and hydrolysis probe CV-A5-P (5′-FAM-CGCAGAGTTCACCTTTATCACCG-BHQ) were used to amplify a 114-bp fragment of the VP1 region. vRNA was extracted from 200 μl of each organ sample using a viral total RNA extraction kit according to the manufacturer's protocol (Shenggong, China). The RNA sample was mixed with other reagents and solutions from a one-step RT-PCR kit (TaKaRa, Japan) in a reaction volume of 25 μl. qRT-PCR was performed with an Applied Biosystems 7500 real-time PCR system (Thermo Fisher Scientific, USA).

Histopathologic and IHC analyses. Tissues were sectioned, fixed, embedded in paraffin, sliced, and stained with hematoxylin by the pathology analysis service of Biofavor Biotech Corporation (China). Immunohistochemical staining was performed according to Biofavor Biotech Company's protocols. Briefly, the paraffinized tissue sections were dewaxed in xylene and rehydrated through immersion in graded concentrations of alcohol. Antigens were retrieved using Trilogy (Cell Marque, Rocklin, CA, USA), and endogenous peroxidase activity was quenched with 3% H_2O_2 in methanol. After washing with PBS, the slides were incubated with a 1:100 dilution of rabbit anti-CV-A5 FP. After primary antibody incubation, CV-A5 antigen was detected using a goat-anti-rabbit secondary antibody and a DAB peroxidase (HRP) substrate kit (Solarbio, China) according to the manufacturer's instructions. The slides were counterstained with hematoxylin stain (Sigma-Aldrich, USA). After washing with PBS and dehydration, sealed slides were examined under a microscope.

Statistical analyses. All statistical analyses were performed using GraphPad Prism 6 software (GraphPad Software Inc., USA). One-way and two-way analysis of variance (ANOVA) with Dunnett's multiple-comparison test were used. The log rank test was applied to compare the survival rates of different groups of mice. A P value of <0.05 was considered significant. Data from animal studies were compiled in Microsoft Excel. Plasmid mapping and primer design were performed using Snap Gene 3.2.1.

ACKNOWLEDGMENTS

We thank Elizabeth Shen Shen for proofreading the manuscript.

We have no conflicts of interest to report.

This work was supported by the Ministry of Science and Technology of the People's Republic of China (no. 2015ZX09102021).

REFERENCES

1. Hu YF, Yang F, Du J, Dong J, Zhang T, Wu ZQ, Xue Y, Jin Q. 2011. Complete genome analysis of coxsackievirus A2, A4, A5, and A10 strains isolated from hand, foot, and mouth disease patients in China revealing frequent recombination of human enterovirus A. J Clin Microbiol 49:2426–2434. https://doi.org/10.1128/JCM.00007-11.
2. Solomon T, Lewthwaite P, Perera D, Cardosa MJ, McMinn P, Ooi MH. 2010. Virology, epidemiology, pathogenesis, and control of enterovirus 71. Lancet Infect Dis 10:778–790. https://doi.org/10.1016/S1473-3099(10)70194-8.
3. Zhang FK, Lu J, Wu J, Wang ZJ, Ji YQ, Zheng XL, Shen S. 2016. Immunogenicity of full and empty particles of coxsackievirus A16. Chin J Biol 28:1132–1137. https://doi.org/10.13200/j.cnki.cjb.001133.
4. Pulli T, Koskimies P, Hyypiä T. 1995. Molecular comparison of coxsackie A virus serotypes. Virology 212:30–38. https://doi.org/10.1006/viro.1995.1450.
5. Flewett TH, Warin RP, Clarke SK. 1963. "Hand, foot, and mouth disease" associated with Coxsackie A5 virus. J Clin Pathol 16:53–55. https://doi.org/10.1136/jcp.16.1.53.
6. Zavate O, Avram G, Pavlov E, Burlea-Iriciuc A, Ivan A, Cotor F. 1984. Coxsackie A virus-associated herpetiform angina. Virologie 35:49–53.
7. Bârlean L, Avram G, Pavlov E, Cotor F. 1994. Investigation of five cases of vesicular enteroviral stomatitis with exanthema induced by coxsackie A5 virus. Rev Roum Virol 45:3–9.
8. Davia JL, Bel PH, Ninet VZ, Bracho MA, González-Candelas F, Salazar A, Gobernado M, Bosch IF. 2011. Onychomadesis outbreak in Valencia, Spain associated with hand, foot, and mouth disease caused by enteroviruses. Pediatr Dermatol 28:1–5. https://doi.org/10.1111/j.1525-1470.2010.01161.x.
9. Pham NTK, Thongprachum A, Trinh QD, Okitsu S, Komine-Aizawa S, Shimizu H, Hayakawa S, Ushijima H. 2018. Detection and genetic characterization of enterovirus strains circulating among children with acute gastroenteritis in Japan during 2014–2016. Infect Genet Evol 61:16–19. https://doi.org/10.1016/j.meegid.2018.03.009.
10. Boros Á, Pankovics P, Kőmíves S, Liptai Z, Dobner S, Ujhelyi E, Várallyay G, Zsidegh P, Bolba N, Reuter G. 2017. Co-infection with coxsackievirus A5 and norovirus GII.4 could have been the trigger of the first episode of severe acute encephalopathy in a six-year-old child with the intermittent form of maple syrup urine disease (MSUD). Arch Virol 162:1757–1763. https://doi.org/10.1007/s00705-017-3299-z.
11. Ji YL, Wang YW. 2012. Analysis on the characteristics of severe hand foot and mouth disease cases and molecular typing of the causative agent. Modern Prev Med 39:2817–2819. https://doi.org/CNKI:SUN:XDYF.0.2012-11-071.
12. D'Angelo A, Ferrante P, Barbi Guidotti M, Provera F. 1983. Influenza B-associated Reye syndrome: report of a case with isolation of a coxsackie A5 virus from CSF. Ital J Neurol Sci 4:329–334. https://doi.org/10.1007/BF02043487.
13. Kon Y, Takahashi S, Takahata N, Onodera I, Sato M. 1974. Case of chronic encephalitis with Coxsackie A5 virus isolated from the cerebrospinal fluid. Rinsho Shinkeigaku 14:752–759.

14. Wang J, Zhou J, Xie G, Zheng S, Lou B, Chen Y, Wu Y. 2020. The epidemiological and clinical characteristics of hand, foot, and mouth disease in Hangzhou, China, 2016 to 2018. Clin Pediatr 59:656–662. https://doi.org/10.1177/0009922820910822.
15. Chen KT, Chang HL, Wang ST, Cheng YT, Yang JY. 2007. Epidemiologic features of hand-foot-mouth disease and herpangina caused by enterovirus 71 in Taiwan, 1998–2005. Pediatrics 120:e244–e252. https://doi.org/10.1542/peds.2006-3331.
16. Wu Y, Yeo A, Phoon MC, Tan EL, Poh CL, Quak SH, Chow VT. 2010. The largest outbreak of hand; foot and mouth disease in Singapore in 2008: the role of enterovirus 71 and coxsackievirus A strains. Int J Infect Dis 14:e1076–e1081. https://doi.org/10.1016/j.ijid.2010.07.006.
17. Fang CY, Liu CC. 2018. Recent development of enterovirus A vaccine candidates for the prevention of hand, foot, and mouth disease. Expert Rev Vaccines 17:819–831. https://doi.org/10.1080/14760584.2018.1510326.
18. Shih C, Liao CC, Chang YS, Wu SY, Chang CS, Liou AT. 2018. Immunocompetent and immunodeficient mouse models for enterovirus 71 pathogenesis and therapy. Viruses 10:674. https://doi.org/10.3390/v10120674.
19. Wang YF, Yu CK. 2014. Animal models of enterovirus 71 infection: applications and limitations. J Biomed Sci 21:31. https://doi.org/10.1186/1423-0127-21-31.
20. McMinn PC. 2002. An overview of the evolution of enterovirus 71 and its clinical and public health significance. FEMS Microbiol Rev 26:91–107. https://doi.org/10.1111/j.1574-6976.2002.tb00601.x.
21. Khong WX, Yan B, Yeo H, Tan EL, Lee JJ, Ng JK, Chow VT, Alonso S. 2012. A non-mouse-adapted enterovirus 71 (EV71) strain exhibits neurotropism, causing neurological manifestations in a novel mouse model of EV71 infection. J Virol 86:2121–2131. https://doi.org/10.1128/JVI.06103-11.
22. Yang B, Chuang H, Yang KD. 2009. Sialylated glycans as receptor and inhibitor of enterovirus 71 infection to DLD-1 intestinal cells. Virol J 6:141. https://doi.org/10.1186/1743-422X-6-141.
23. Liu J, Dong W, Quan X, Ma C, Qin C, Zhang L. 2012. Transgenic expression of human p-selectin glycoprotein ligand-1 is not sufficient for enterovirus 71 infection in mice. Arch Virol 157:539–543. https://doi.org/10.1007/s00705-011-1198-2.
24. Zhang W, Dai W, Zhang C, Zhou Y, Xiong P, Wang S, Ye X, Liu Q, Zhou D, Huang Z. 2018. A virus-like particle-based tetravalent vaccine for hand, foot, and mouth disease elicits broad and balanced protective immunity. Emerg Microbes Infect 7:94. https://doi.org/10.1038/s41426-018-0094-1.
25. Cai Y, Ku Z, Liu Q, Leng Q, Huang Z. 2014. A combination vaccine comprising of inactivated enterovirus 71 and coxsackievirus A16 elicits balanced protective immunity against both viruses. Vaccine 32:2406–2412. https://doi.org/10.1016/j.vaccine.2014.03.012.
26. Zhang Z, Dong Z, Wei Q, Carr MJ, Li J, Ding S, Tong Y, Li D, Shi WF. 2017. A neonatal murine model of coxsackievirus A6 infection for evaluation of antiviral and vaccine efficacy. J Virol 91:e02450. https://doi.org/10.1128/JVI.02450-16.
27. Yang L, Mao Q, Li S, Gao F, Zhao H, Liu Y, Wan J, Ye X, Xia N, Cheng T, Liang Z. 2016. A neonatal mouse model for the evaluation of antibodies and vaccines against coxsackievirus A6. Antiviral Res 134:50–57. https://doi.org/10.1016/j.antiviral.2016.08.025.
28. Shen C, Liu Q, Zhou Y, Ku Z, Wang L, Lan K, Ye X, Huang Z. 2016. Inactivated coxsackievirus A10 experimental vaccines protect mice against lethal viral challenge. Vaccine 34:5005–5012. https://doi.org/10.1016/j.vaccine.2016.08.033.
29. Zhang Z, Dong Z, Li J, Carr MJ, Zhuang D, Wang J, Zhang Y, Ding S, Tong Y, Li D, Shi W. 2017. Protective efficacies of formaldehyde-inactivated whole-virus vaccine and antivirals in a murine model of coxsackievirus A10 infection. J Virol 91:e00333. https://doi.org/10.1128/JVI.00333-17.
30. Zhang Z, Dong Z, Wang Q, Carr MJ, Li J, Liu T, Li D, Shi WF. 2018. Characterization of an inactivated whole-virus bivalent vaccine that induces balanced protective immunity against coxsackievirus A6 and A10 in mice. Vaccine 36:7095–7104. https://doi.org/10.1016/j.vaccine.2018.09.069.
31. Zhang Z, Zhang X, Carr MJ, Zhou H, Li J, Liu S, Liu T, Xing W, Shi WF. 2019. A neonatal murine model of coxsackievirus A4 infection for evaluation of vaccines and antiviral drugs. Emerg Microbes Infect 8:1445–1455. https://doi.org/10.1080/22221751.2019.1673135.
32. Wiegers KJ, Yamaguchi-Koll U, Drzeniek R. 1977. Differences in the physical properties of dense and standard poliovirus particles. J Gen Virol 34:465–473. https://doi.org/10.1099/0022-1317-34-3-465.
33. Yamaguchi-Koll U, Wiegers KJ, Drzeniek R. 1975. Isolation and characterization of "dense particles" from poliovirus-infected HeLa cells. J Gen Virol 26:307–319. https://doi.org/10.1099/0022-1317-26-3-307.
34. Wetz K, Zeichhardt H, Willingmann P, Habermehl KO. 1983. Dense particles and slow sedimenting particles produced by ultraviolet irradiation of poliovirus. J Gen Virol 64:1263–1275. https://doi.org/10.1099/0022-1317-64-6-1263.
35. Boublik M, Drzeniek R. 1976. Demonstration of a core in poliovirus particles by electron microscopy. J Gen Virol 31:447–449. https://doi.org/10.1099/0022-1317-31-3-447.
36. Wiegers KJ, Yamaguchi-Koll U, Drzeniek R. 1976. A complex between poliovirus RNA and the structural polypeptide VP1. Biochem Biophys Res Commun 71:1308–1312. https://doi.org/10.1016/0006-291x(76)90797-x.
37. He M, Xu L, Zheng Q, Zhu R, Yin Z, Zha Z, Lin Y, Yang L, Huang Y, Ye X, Li S, Hou W, Wu Y, Han J, Liu D, Li Z, Chen Z, Yu H, Que Y, Wang Y, Yan X, Zhang J, Gu Y, Zhou ZH, Cheng T, Li S, Xia N. 2020. Identification of antibodies with non-overlapping neutralization sites that target coxsackievirus A16. Cell Host Microbe 27:1–13. https://doi.org/10.1016/j.chom.2020.01.003.
38. Wen X, Sun D, Guo J, Elgner F, Wang M, Hildt E, Cheng A. 2019. Multifunctionality of structural proteins in the enterovirus life cycle. Future Microbiol 14:1147–1157. https://doi.org/10.2217/fmb-2019-0127.
39. Standardization Administration of China. 2018. Laboratory animal—guideline for ethical review of animal welfare. Standardization Administration of China, Beijing, China.
40. Hankaniemi MM, Laitinen OH, Stone VM, Sioofy-Khojine A, Määttä JAE, Larsson PG, Marjomäki V, Hyöty H, Flodström-Tullberg M, Hytönen VP. 2017. Optimized production and purification of coxsackievirus B1 vaccine and its preclinical evaluation in a mouse model. Vaccine 35:3718–3725. https://doi.org/10.1016/j.vaccine.2017.05.057.
41. Jin WP, Lu J, Wu J, Hu G, Zhou JG, Wang WH, Wang ZJ, Meng SL, Shen S. 2020. Prokaryotic expression and polyclonal antibody preparation of coxsackievirus A5 VP1. Int J Biol 43:53–57. https://doi.org/10.3760/cma.j.cn311962-20191118-00063.
42. Hu YX, Guo JY, Shen L, Chen Y, Zhang ZC, Zhang YL. 2002. Get effective polyclonal antisera in one month. Cell Res 12:157–160. https://doi.org/10.1038/sj.cr.7290122.